Costa *et al. J Artif Intell Smart Energy Syst* *(2026) 5:61*
https://doi.org/10.68159/e352554475

ORIGINAL RESEARCH **Open access**

Optimized FOPID-Based Load Frequency Control in Single and Dual-Area Microgrids

Helena Costa[1*], Rui Martins[1], Bruno Lopes[2], Ana Ferreira[1]

Abstract

Energy management architectures of tomorrow will heavily rely on microgrid technologies. When properly integrated and implemented, these localized grids can secure energy autonomy for countless regions. However, a microgrid's overall success is fundamentally tethered to how reliably and stably it operates. In this context, fractional control schemes present highly viable methodologies for safeguarding operational stability. In this manuscript, a secondary load frequency control (LFC) framework driven by a fractional-order proportional–integral–derivative (FOPID) algorithm is introduced for application in both single- and dual-area AC microgrid networks. To establish the five crucial gain parameters of these fractional PID units, cohort intelligence (CI) optimization is utilized. The operational efficacy of this CI-calibrated FOPID mechanism is subsequently evaluated against standard PID modules—calibrated via genetic algorithm (GA) and particle swarm optimization (PSO)—using identical single- and dual-area test systems. To thoroughly gauge LFC capabilities and contrast the distinct regulatory and tuning mechanisms, the study models four unique AC microgrid scenarios. The initial scenario investigates demand shifts within a single-area AC network, both incorporating and excluding distributed energy resources. A second scenario analyzes load shifts across an interconnected two-area AC setup. The final two scenarios investigate the impacts of stochastic step-load fluctuations and parametric system variations, respectively. The core findings confirm that the CI-optimized FOPID mechanism outperforms the GA- and PSO-calibrated PID models, demonstrating enhanced steady-state accuracy when measured against the Integral Time Absolute Error (ITAE) objective criterion.

Keywords Genetic algorithm, Particle swarm optimization, Load frequency control, Cohort intelligence, Fractional order PID controller

*Correspondence:
Helena Costa
helena.costa@up.pt
[1] Department of Artificial Intelligence in Energy Engineering, Faculty of Engineering, University of Porto, Porto, Portugal
[2] Department of Smart Grid Analytics, Faculty of Engineering, University of Lisbon, Lisbon, Portugal

Introduction

For both utility providers and end-users within the power industry, microgrid systems represent an exceptionally practical solution for power management. Depending on specific power traits and voltage levels, these localized networks are broadly categorized into pure DC, pure AC, or hybrid AC/DC configurations. Specifically, an AC microgrid is engineered to operate autonomously in geographic zones suffering from total grid blackouts or inadequate energy deliveries from overarching utility networks. Furthermore, it is heavily anticipated that diverse decentralized energy assets—including freezer systems, heat pumps, and electric transport—must operate seamlessly despite any erratic spikes or drops in power generation or usage. The widespread public adoption of plug-in electric vehicles has notably curtailed fossil fuel dependency and related greenhouse gas emissions, significantly advancing ecological sustainability. To ensure power delivery remains both economically viable and qualitatively sound from the generator to the end-user, LFC is absolutely

This is an open access article distributed under the terms of the Creative Commons Attribution-NonCommercial-ShareAlike 4.0 International License (CC BY-NC-SA 4.0), which permits non-commercial use, distribution, reproduction, and adaptation in any medium or format, provided that appropriate credit is given to the original author(s) and source, a link to the license is provided, and any changes made are indicated. Adapted material must be distributed under the same license.

© 2026 The Author(s). | Published by Institute of Smart Energy Systems Press

critical. Any shifts in power demand mandate immediate recalibration of the AC microgrid's operational state. Such demand volatility forces the system's frequency away from its nominal values, pushing the grid toward instability. Consequently, the primary mandate of LFC mechanisms is to preserve this nominal frequency—or at least contain deviations within secure margins—by dictating generator outputs via a dual-loop framework: a primary mechanical input regulator and a secondary or auxiliary controller. Historically, basic integral (I), PI, or PID architectures have been deployed as this secondary LFC tier to achieve static accuracy while curbing adverse transient behaviors during frequency stabilization. However, legacy calibration methodologies like Ziegler-Nichols or rudimentary trial-and-error fail to adequately govern the highly nonlinear dynamics and shifting operational conditions inherent to microgrid networks [1].

To appropriately calibrate AC microgrid LFC modules, the academic community has proposed an extensive array of optimal heuristic search techniques, such as the genetic algorithm [2], the difference vector method [3], ant colony optimization (ACO) [4-6], particle position and velocity schemes [7], teaching-learning-based optimization [8, 9], grey wolf optimization [10], flower pollination algorithms (FPO) [11], artificial bee colony architectures (ABC) [12], and various other biologically inspired metaheuristics [13]. In parallel, investigators have probed alternative regulatory paradigms for frequency stabilization, including fuzzy logic systems [14-16], artificial neural networks [17], and adaptive neuro-fuzzy frameworks (ANFIS) [18]. For the explicit purpose of managing frequency across a tripartite microgrid layout, certain scholars have heavily endorsed two-degree-of-freedom iterations of I, PI, and PID controllers [19-21]. Despite the successful maturation of highly advanced regulatory models, the vast majority of deployed industrial solutions rely on fundamental PI or PID structures. Their persistent dominance is attributed to their structural minimalism, high resilience, broad applicability, and seamless availability across analog and digital platforms. Furthermore, extensive scholarly focus has been dedicated to ensuring proficient control of diverse linear, highly nonlinear, and fractional-order topologies [22-27].

More recently, fractional order (FO) mechanisms have emerged as the preferred regulatory choice within LFC deployments [28-32]. Fundamentally, the FOPID architecture is an evolutionary step beyond the classic PID setup, achieved through the application of fractional calculus. Alongside the standard Kp, Ki, and Kd coefficients, the FOPID framework introduces two supplementary design constraints, λ and μ, thereby expanding the multidimensional search space for defining optimal controller gains. Previous studies have successfully mathematically represented the FOPID unit by mirroring the integer-order classic PID layout alongside its analog equivalents utilizing capacitive, inductive, and resistive elements [33]. The prominent advantages of deploying FOPID architectures include reduced steady-state inaccuracies, enhanced robustness—specifically characterized by immunity to shifting system states—and heightened dynamic resilience when subjected to minor signal disturbances. Parallel research has also validated the FOPID module acting as a supplementary regulatory unit within the LFC of hybrid energy networks [34]. Furthermore, independent scholars have seamlessly integrated fractional-order fuzzy logic mechanisms into mixed-generation grids that incorporate renewable energy assets [35].

The current investigation deploys a fractional-order control scheme within a single-area AC microgrid that features the decentralized governance of a freezer unit, a thermal heat pump, and an electric vehicle. The specific coefficients of this fractional controller—Kp, Ki, Kd, λ, and μ—were mapped as mathematical objective functions, with their ideal absolute configurations determined via the CI algorithmic approach [36-39]. The remainder of this manuscript is structured systematically. The mathematical formulation of the proposed AC microgrid is first outlined, followed by a concise overview of both socially-driven and naturally-inspired metaheuristics. Subsequently, the fractional calculus principles and the specific LFC mechanism utilized are presented in detail [40]. The empirical outcomes are then presented alongside comprehensive analytical discussions of system efficacy. Ultimately, the primary innovation of this research is rooted in its exhaustive robustness and operational assessments, directly contrasting the CI-calibrated FOPID against GA/PSO-driven PID setups across a wide spectrum of LFC scenarios. These diverse testing conditions encompass load fluctuations (with and without distributed energy assets), randomized step-load disturbances, and parametric shifts across single- and dual-area AC microgrid environments.

© 2026 The Author(s). | Published by Institute of Smart Energy Systems Press

System Modeling, Particle Swarm Optimization and Cohort Intelligence

System modeling

Fundamentally, any physical process can be mathematically mapped using foundational governing laws, analogous to classic mass-balance formulations. Alternatively, data-driven empirical models can be synthesized directly from observed system inputs and their resultant output behaviors. Driven by the explosive growth of advanced data analytics and modern sensor networks, researchers now have access to unprecedented volumes of such input-output datasets. **Figure 1** illustrates the overarching Simulink schematic developed for this research, depicting a single-area microgrid that integrates a conventional thermal power generation plant with localized domestic loads—namely freezer setups, thermal heat pumps, and electric transport—further augmented by measurement delay blocks and washout filters.

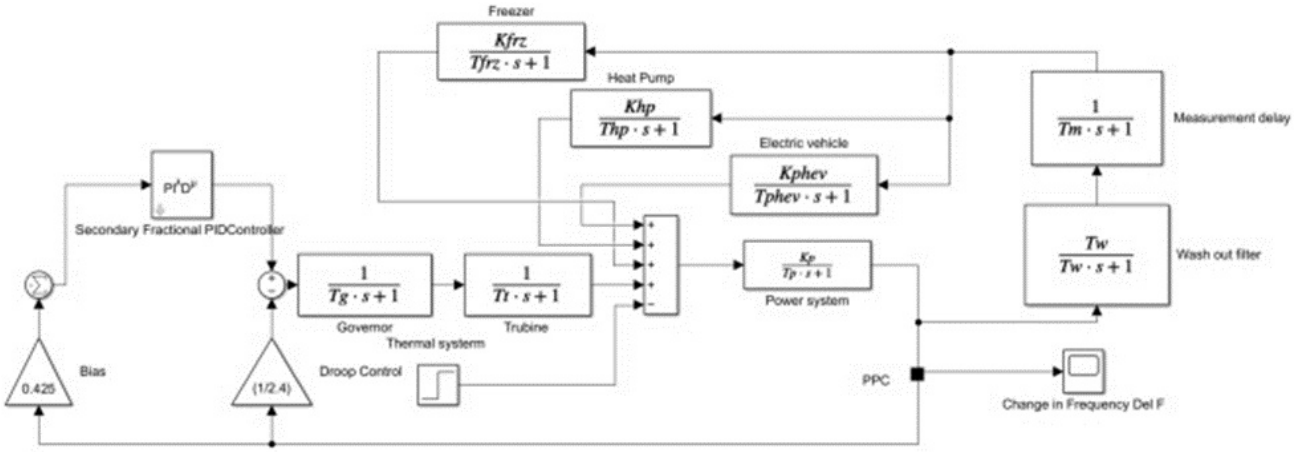


Figure 1. Dynamics of a single-area AC microgrid thermal power scheme with DES.

Genetic algorithm

Throughout this investigation, a genetic algorithm (GA) was applied to isolate the absolute best configuration for the PID operational constants: K_P, K_I and K_D. The GA mechanism calculates a specific fitness metric for each individual 'chromosome' contained in the starting population—which essentially represent the preliminary mathematical guesses constrained strictly by defined minimum and maximum limits. As the algorithm progresses, a subsequent generation is spawned during each cycle, heavily influenced by the cost function evaluations derived from the preceding loop. Following the completion of the mutation, crossover, and survival phases within the ith cycle, the most robust resulting candidate is mathematically represented as $i = [K_P, i, K_I, i, K_D, i]$.

The operational sequence of the GA computational technique is detailed below:

1. Stochastically generate the starting candidate pool denoted by $N(N_p = 5)$

2. Halt the computational process if a pre-established stopping condition is satisfied; if not, advance directly to step 3

3. Evaluate the specific fitness metric for the candidates produced in the present cycle (via simulation runs and ITAE objective analysis)

4. Isolate a parental subset (from the preceding generation's pool) for mutation (utilizing a mutation probability factor of $((P_m) = 0.1)$) and crossover procedures, while executing a tournament-style selection to determine which candidates

© 2026 The Author(s). | Published by Institute of Smart Energy Systems Press

survive intact without modifying the accuracy vector

5. Synthesize novel 'offspring' derivations from the 'parental' units manipulated during the prior phase via standard mutation and crossover protocols

6. Formulate the updated candidate array (combining offspring derived from crossed-over parents + offspring from mutated parents + the baseline population)

7. Loop back to step 2

To quantify performance, the Area Control Error (ACE) was utilized as the primary fitness benchmark across both the isolated single-area and the interconnected dual-area AC microgrid topologies, mathematically articulated below in **Eqs. 1 and 2**, respectively.

$$\mathrm{ACE} = \mathrm{ITAE} = \int_0^t t(|\Delta f|)dt \qquad (1)$$

$$\mathrm{ACE} = \mathrm{ITAE} = \int_0^t t\left(\left|\Delta f_1\right| + \left|\Delta f_{12}\right| + \left|\Delta P_{tie}\right|\right) dt \qquad (2)$$

Particle swarm optimization

Initially conceptualized in 1995, Particle Swarm Optimization (PSO) operates as an ecologically driven computational strategy. It isolates ideal solution vectors by tracking and analyzing the simulated kinematics of a particle cluster [7]. Fundamentally, a computational swarm conceptually mirrors the collective biological movements seen in avian flocks, apiary colonies, ant hills, or marine schools. Specifically, the mechanical foundation of PSO is heavily derived from the synchronized flight patterns of flocking birds. The updated spatial coordinate vector Xi (t+1) of a given entity, alongside its respective trajectory vector Vi (t+1), are mathematically computed via **Eqs. 3 and 4**. Within these expressions, Xi (t) and Vi (t) denote the foundational spatial and velocity coordinates of individual entities navigating the multidimensional search matrix. Furthermore, the variables c_1, c_2, and r_1, r_2 correspond to customized acceleration constants and randomized numerical inputs, respectively [12]. The operational sequence of the PSO computational technique is detailed below:

1. Stochastically assign the foundational spatial coordinates and movement velocities for the entire particle collective

2. Compute the precise objective function score for every individual entity

3. Identify the spatial coordinate that yields the highest historical fitness score for each distinct unit, designating this metric as the personal best (Pbest) of that particle

4. Isolate the absolute highest-performing coordinate from the collective Pbest repository, cementing it as the Global best (Gbest)

5. Recalculate **Eqs. 3 and 4** utilizing the newly established Gbest coordinates

$$V_i^{(t+1)} = X_i^{(t)} + c_1 r_1 \left(P_{\mathrm{best}i} - X_i^{(t)}\right) + c_2 r_2 \left(G_{\mathrm{best}i} - X_i^{(t)}\right) \qquad (3)$$

© 2026 The Author(s). | Published by Institute of Smart Energy Systems Press

$$X_i^{(t+1)} = X_i^t + V_i^{(t+1)} \quad (4)$$

6. Terminate the computational loop and lock in the active global best coordinate as the definitive final solution if a pre-set stopping parameter is triggered; conversely, cycle back to step 2

Cohort intelligence

The CI framework identifies the ideal system modeling parameters by seeking the minimum integral time absolute error. It improves the objective function's fitness value through continuous interaction and competitive behavior among distinct candidate solutions, known as cohorts. In this research, the efficacy of cohort intelligence is evaluated against particle swarm optimization and genetic algorithms in calibrating both traditional PID and fractional-order PID units. The dynamics of the two-area AC microgrid thermal power system are presented in **Figure 2**. **Figure 3** illustrates the operational flowchart of the CI methodology. To begin, the user-specified variables for the Cohort Intelligence framework were adopted from existing literature [38], detailed in **Table 1**. The CI technique was programmed using MATLAB 2014a, running on a Windows 10 Home Basic system equipped with an AMD PRO A4 processor and 4 GB of RAM, utilizing the FOMCON toolbox to optimize the FOPID controller gains. The parameter r **(Table 1)** is typically designated between 0.9 and 1 to facilitate more rapid convergence. The operational sequence of the CI methodology proceeds as follows:

1. Initially, random design metrics (Cohort characters) are generated for each cohort, strictly confined within the user-specified minimum and maximum limits.

2. Next, these design attributes (Cohort characters) are evaluated across all cohorts to establish fitness functions based on integral time absolute errors.

3. The probability that another will follow one Cohort is dictated by their respective fitness scores. A Cohort demonstrating a superior fitness function is naturally pursued by the rest.

4. Every Cohort updates its fitness metrics by systematically adjusting the upper and lower boundaries.

5. The algorithm's convergence is ultimately triggered either by reaching the maximum allowed iteration count or by observing minimal discrepancy among the Cohort characters.

Table 1. Algorithm parameters for CI.

Parameter	Assigned value
Number of decision variables (N)	5
Number of cohorts (C)	3
Saturation/Convergence criterion (ε)	0.000001
Interval reduction coefficient (r)	0.97

Fractional Calculus/Fractional PID Controller

Fractional calculus

© 2026 The Author(s). | Published by Institute of Smart Energy Systems Press

Fractional calculus has been the subject of investigation for over 300 years due to its wide-ranging utility across various scientific and engineering domains. Its foundational methodology relies on the integrals and derivatives of positive real numbers. Fractional mathematics was initially introduced by N. Abel in 1823, who determined that the integral mathematical expression for the tautochrone problem could yield a result of 0.5. The systematic exploration of fractional mathematics was subsequently formalized by J. Liouville in 1832. Later, in 1990, M. Axtell demonstrated the application of fractional mathematics for executing specific operations within control systems, introducing the deployment of diverse integral operators via the Laplace transformation. He advocated for a comprehensive investigation into fractional mathematics within control engineering to fully understand its implications. Multiple formal definitions of fractional calculus have been established by prominent scholars, including Grunwald, Riemann, and M. Caputo, who thoroughly analyzed the systematic frameworks underlying fractional calculus [2, 12, 16, 20, 21, 28-30]. These foundational definitions are summarized below:

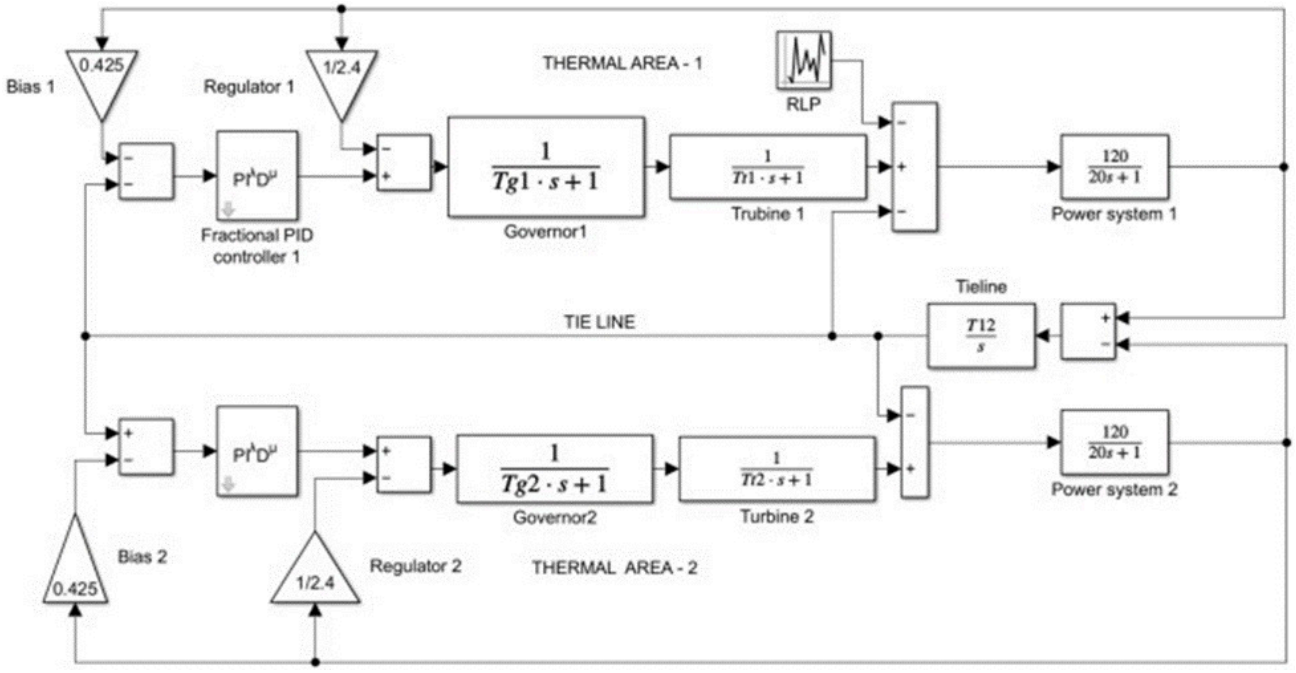
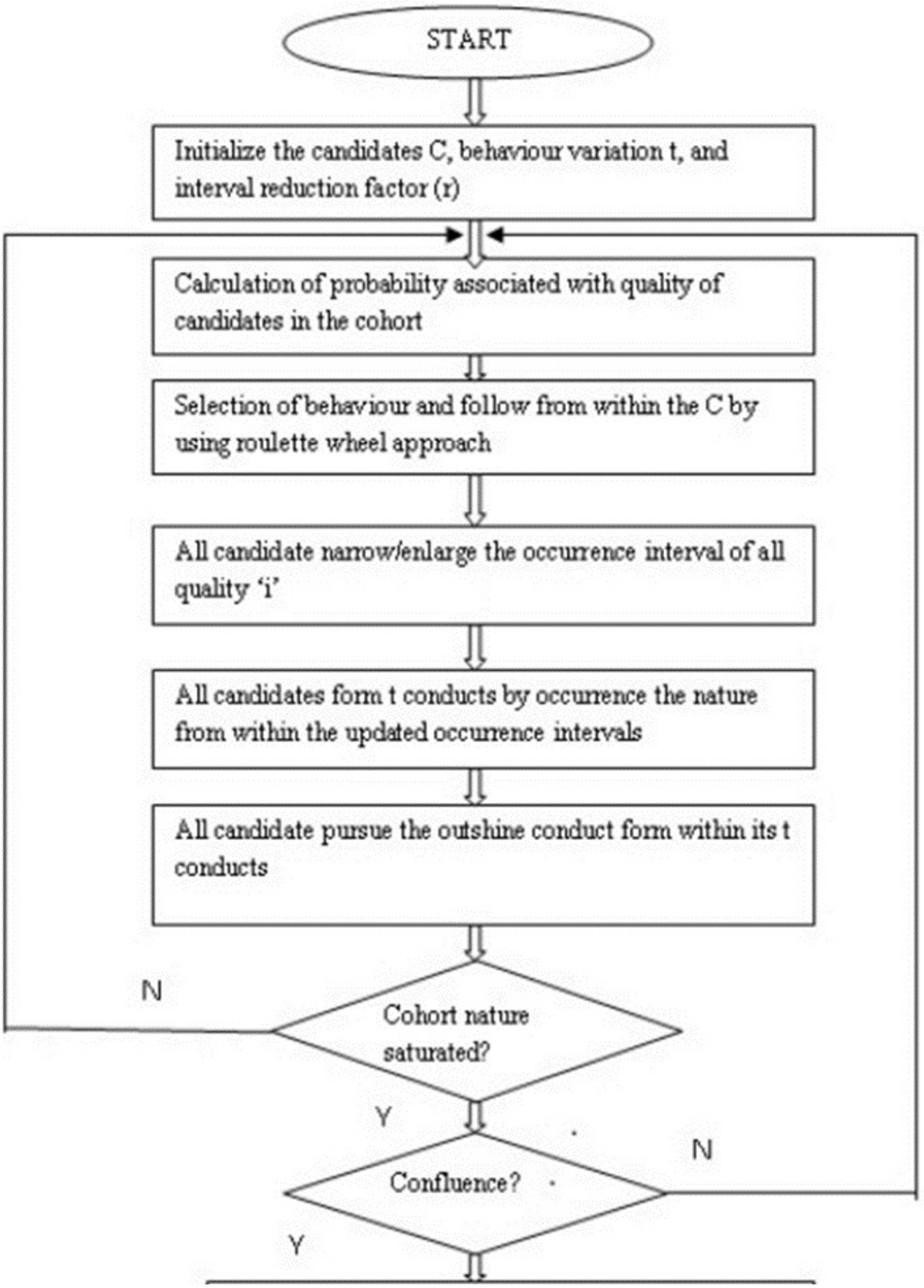
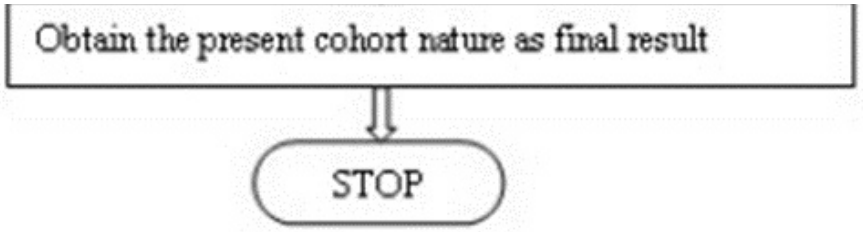


Figure 2. Dynamics of two areas AC microgrid thermal power system.

© 2026 The Author(s). | Published by Institute of Smart Energy Systems Press



© 2026 The Author(s). | Published by Institute of Smart Energy Systems Press



$$ {}_aD_t^{\alpha} = \lim_{h \to 0} \frac{1}{h^{\alpha}} \sum_{r=0}^{\left[\frac{t-a}{h}\right]} (-1)^r \binom{n}{r} f(t - rh) \quad (5) $$

Where n denotes an integer, a and t serve as the operational bounds, $\left[\frac{t-a}{h}\right]$ indicates the integer portion, and α is constrained by n - 1 < α < n. Furthermore, nr represents the binomial coefficient, formulated as follows:

$$ \binom{n}{r} = \frac{\Gamma(n+1)}{\Gamma(r+1)\Gamma(n-r+1)} \quad (6) $$

Within the preceding expression, the Gamma function is defined as:

$$ \Gamma(x) = \int_0^{\infty} t^{x-1} e^{-t} dt, \Re(Z) > 0 \quad (7) $$

Riemann–Liouville definition

The Riemann–Liouville formulation utilizes fractional operators to resolve differential equations and integrate non-integer values. It is mathematically articulated as:

$$ {}_aD_t^{\alpha} = D^n J^{n-\alpha} f(t) = \frac{1}{\Gamma(n-\alpha)} \left(\frac{d}{dt}\right)^n \int_a^t \frac{f(\tau)}{(t-\tau)^{\alpha-n+1}} d\tau \quad (8) $$

Where n represents an integer, α denotes a real number bounded by -1 < α < n, J acts as the integral operator, and t and a define the integration limits.

M. Caputo definition

The M. Caputo formulation permits standard initial conditions like y(0) and y′(0), contrasting with purely fractional initial states such as y0.5(0). This approach is highly favored within the engineering community because it allows the initial conditions to correlate directly with the specific nature of the applied fractional derivatives. It is described mathematically as:

$$ {}_aD_t^{\alpha} = \frac{1}{\Gamma(n-\alpha)} \int_a^t \frac{f^n(\tau)}{(t-\tau)^{\alpha-n+1}} d\tau \quad (9) $$

© 2026 The Author(s). | Published by Institute of Smart Energy Systems Press

Where n signifies an integer, α is a real number restricted to -1 < α < n, J functions as the integral operator, and t and a serve as the boundaries for integration.

Investigators have probed a variety of analytical techniques to secure stable and accurate solutions for exact, singular, and conformable nonlinear fractional differential equations, which are highly relevant for diverse control mechanisms [41-45].

Fractional PID controller

I. Podlubny introduced and popularized the fractional PID controller for fractional-order control architectures in 1994. Following its inception, researchers integrated the fractional-order PID controller across multiple disciplines employing varied tuning and design strategies. The fundamental mathematical principles of fractional calculus, alongside its architectural implementation for the fractional PID controller, are illustrated in **Figure 4**. Calibrating a FOPID controller is inherently challenging due to the presence of two extra parameters that must be configured, contrasting with the standard three-parameter PID setup. Within the FOPID framework, the derivative and integral operations share a fractional order. Consequently, in addition to the standard proportional, integral, and derivative constants K_p, K_i, and K_d, the FOPID structure introduces two supplementary gains: the positive real non-integer variables λ and μ. To successfully manage a specific process via a FOPID unit, precise optimal values must be identified for K_p, K_i and K_d, λ, and μ. Therefore, tuning FOPID parameters necessitates navigating a five-dimensional optimization hyperspace. During this calibration process, the proportional, integral, and derivative constants are typically bounded between 0 and 10, whereas the λ and μ variables are restricted between 0 and 2. Academics have investigated extensive use-cases for FOPID mechanisms, spanning closed-loop operations in nanocomposite manufacturing [46-48], power electronics [49, 50], bolted joint assemblies [51], DC motors [52], and non-minimum phase processes [53]. Furthermore, comprehensive literature reviews [54, 55] have systematically cataloged the prominent advancements and evolving research trajectories concerning FOPID controllers.

Figure 4 displays the standard architectural layout of a FOPID controller. This device distinguishes itself from the classic PID mechanism by offering a greater number of tunable parameters. This distinct characteristic enables the FOPID to secure highly stable regulation over the AC microgrid framework. As a result, the $\mathrm{PI}^{\lambda}\mathrm{D}^{\mu}$ configuration of the FOPID is anticipated to bolster overall system dynamics. Nevertheless, effectively tuning the fractional PID controller remains a primary challenge during the design phase. The overarching transfer function for this controller is expressed below:

$$\mathrm{FOPID} = U(s) = K_P + \frac{K_D}{s^{\lambda}} + K_D s^{\mu} \quad (10)$$

Where KP represents the proportional gain, K_I is the integral gain, K_D denotes the derivative gain, λ signifies a positive real non-integer value (representing the integration order), and μ indicates a positive real non-integer value (representing the differentiation order).

© 2026 The Author(s). | Published by Institute of Smart Energy Systems Press

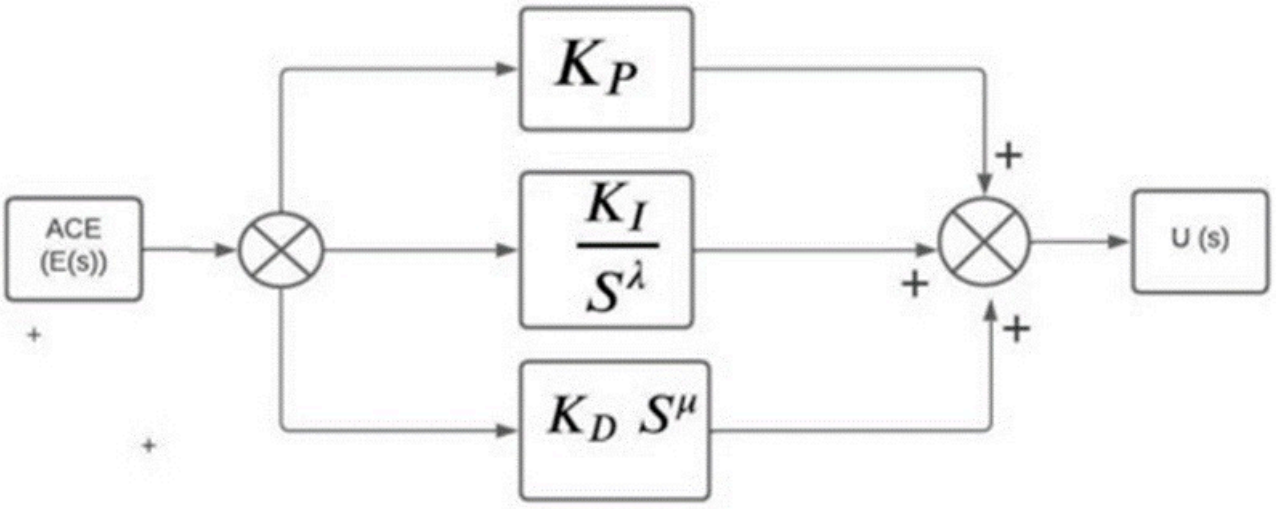


Figure 4. General structure of FOPID regulator.

For the present investigation, five specific gain metrics were computationally optimized to model the fractional-order proportional-integral-derivative controller within the targeted AC microgrid architecture. By assigning (λ, μ) values of (1, 1) for standard PID, (1, 0) for PI, (0, 1) for PD, and (0, 0) for a standalone P controller, the classical PID controller domain is graphically represented in **Figure 5**. This illustration demonstrates how the operational search space of the fractional-order controller extends significantly beyond the rigid coordinate points of the conventional PID plane. This expanded search domain provides enhanced flexibility and auxiliary advantages when configuring FOPID controllers, ultimately yielding higher precision in system outputs. The elevated efficacy of the FOPID compared to the classic PID within the designated AC microgrid framework is realized by meticulously tuning all five design parameters (K_p, K_i, K_d, λ, μ). This calibration ensures seamless iso-damping characteristics alongside the resilient and stable management of nonlinear system behaviors.

© 2026 The Author(s). | Published by Institute of Smart Energy Systems Press

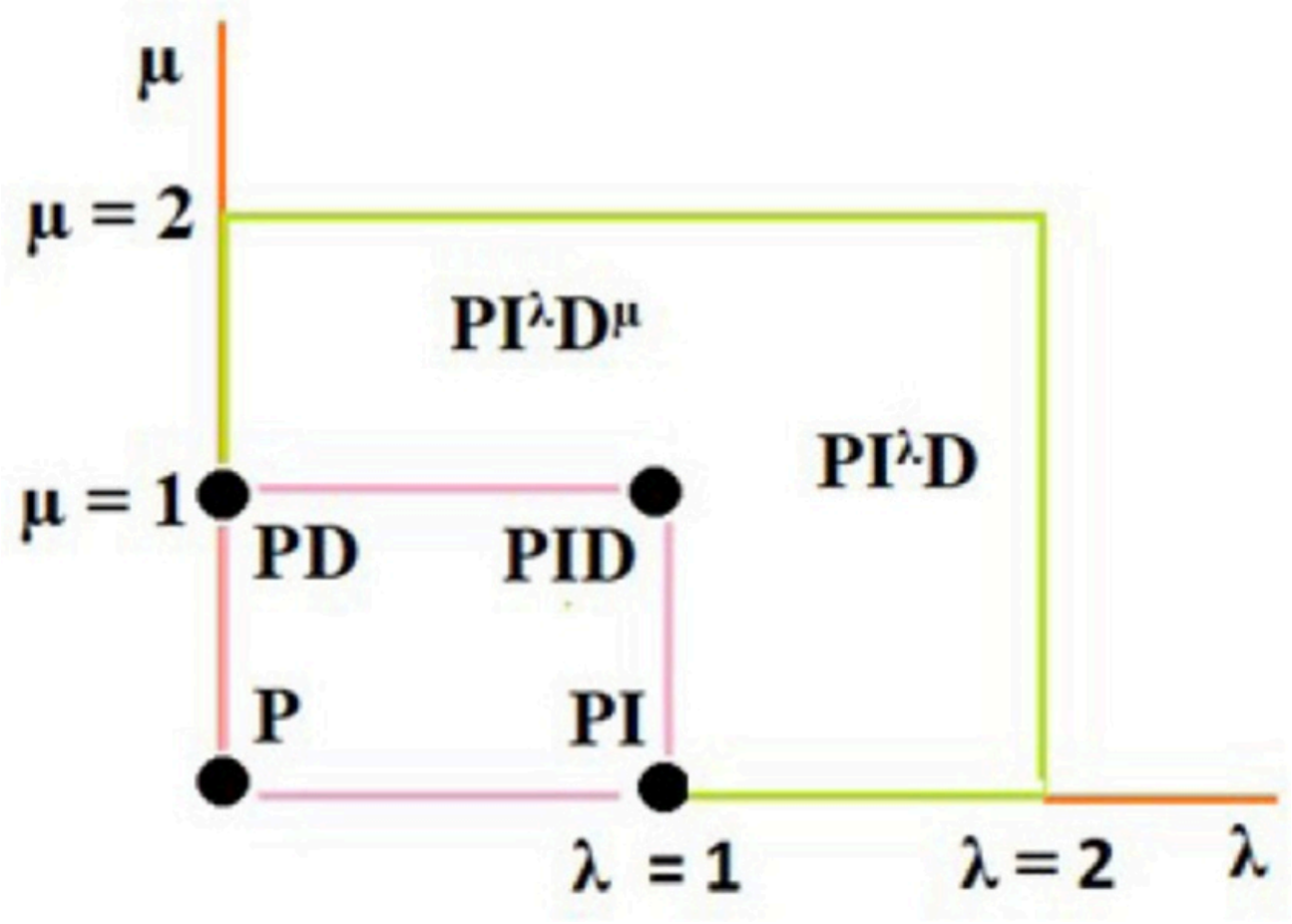


Figure 5. FOPID and conventional PID controller planes.

Results and Discussion

The specific Matlab/Simulink architectural models for the suggested FOPID-based LFC systems, applied to single- and dual-area AC microgrid networks, are depicted in **Figures 1 and 2**, respectively. To properly assess the dynamics of the proposed AC microgrid frameworks, comparative LFC units were additionally modeled utilizing PID controllers optimized via PSO and GA methodologies. Comprehensive microgrid simulations for both single- and dual-area configurations were executed at the Point of Common Coupling (PCC), incorporating variable disruptions such as standard step-load and randomized step-load fluctuations. The operational proficiency of each controller was judged based on response settling times and iso-damping capabilities. **Tables 2 and 3** detail the optimal gain configurations derived from the various soft-computing algorithms—including CI, PSO, and GA—for both the proposed FOPID and the standard PID controllers.

To analyze the transient dynamics of the single-area AC microgrid, the system frequency was subjected to a load perturbation of 0.01 p.u. MW. **Table 2** outlines the steady-state accuracy metrics for the single-area AC microgrid under these specific load shifts. These findings highlight that the response settling times for the single-area network are 6.5 s, 10.5 s, and 4.8 s when using the GA-PID, PSO-PID, and FOPID-driven LFC models, respectively. Concurrently, the respective settling durations for the two-area AC microgrid—specifically observed in area 1 (Δf1), area 2 (Δf2), and the tie-line (ΔPtie12) during step-load variations—are systematically documented in **Table 4.**

© 2026 The Author(s). | Published by Institute of Smart Energy Systems Press

Table 2. Optimized gain values and time domain specifications of single area AC microgrid system without considering DES.

Algorithm	Controller gain values					ITAE	Maximum overshoot	Minimum overshoot	Settling time
Empty Cell	K_P	K_I	K_D	λ	μ	(Error)	(Hz, pu)	(Hz, pu)	(s)
GA-PID	0.4231	0.9852	0.39915	1	1	0.02284	0.00027	−0.019	6.5
PSO-PID	0.6784	1.0000	0.4702	1	1	0.02658	0	−0.017	10.5
FOPID	4.2369	8.7183	3.0103	0.9909	0.7020	0.02567	0.0015	−0.0085	4.8

Table 3. Optimized gain values of two areas AC microgrid system without considering the distributed energy system.

Algorithm	Controller gain values of area 1					Controller gain values of area 2				
	K_{P1}	K_{I1}	K_{D1}	λ_1	μ_1	K_{P2}	K_{I2}	K_{D2}	λ_2	μ_2
GA-PID	0.99896	0.98534	0.39767	1	1	0.96766	0.99931	0.19199	1	1
PSO-PID	0.7129	1.00000	0.5129	1	1	0.7129	1.00000	0.5129	1	1
CI-FOPID	1.6814	3.6597	6.0687	0.9957	0.8971	8.3235	2.8521	4.6309	0.6893	0.9067

Comprehensive assessments of controller iso-damping characteristics are additionally provided in **Table 2 and Table 4**. These empirical outcomes verify that the introduced FOPID controller achieves a substantial reduction in both peak overshoots and undershoots when compared against its PSO-PID and GA-PID counterparts. To rigorously evaluate the AC microgrid simulations, several distinct operational scenarios were analyzed as detailed below:

Table 4. Time domain specifications of a two-area microgrid system without considering the distributed energy system.

Control areas	Algorithm/Controller		ITAE (error)	Maximum overshoot (Hz, pu)	Maximum undershoot (Hz, pu)	Settling time (s)
Two areas		Δ_{F1}		0.003	−0.016	12
	GA-PID	Δ_{F2}	0.02325	0.0012	−0.0045	18
		ΔP_{tie}		0.000105	−0.0022	17
		Δ_{F1}		0.002	−0.0155	18
	PSO-PID	Δ_{F2}	0.03171	0.000466	−0.0041	22
		Δ_{tie12}		0.0003	−0.00228	20
		Δ_{F1}		0.001	−0.0051	15
	CI-FOPID	Δ_{F2}	0.03986	0.00026	−0.0011	20

© 2026 The Author(s). | Published by Institute of Smart Energy Systems Press

		ΔP_{tie}		0.000152	−0.000562	22

Case 1. Load changes in single area AC microgrid with and without distributed energy system (DES)

For the initial scenario, the analysis incorporated a step-load disturbance applied to a 20 MW capacity network (representing 0.01 p.u. MW in the equivalent per-unit system). The resulting frequency deviations within the isolated single-area microgrid (Δf), triggered by this 0.01 p.u. MW load shift, are illustrated in **Figure 6** (excluding DES) and **Figure 7** (incorporating DES). Observing **Figure 6** reveals unequivocally that the FOPID controller delivers superior dynamic behavior, suppressing oscillations and achieving the targeted nominal frequency within a brisk 4.8 s, significantly outpacing the PSO- and GA-calibrated PID mechanisms. Moreover, **Figure 7** confirms that the single-area microgrid augmented with a distributed energy network is similarly regulated with high efficacy by the FOPID unit, maintaining highly acceptable settling times and oscillatory limits.

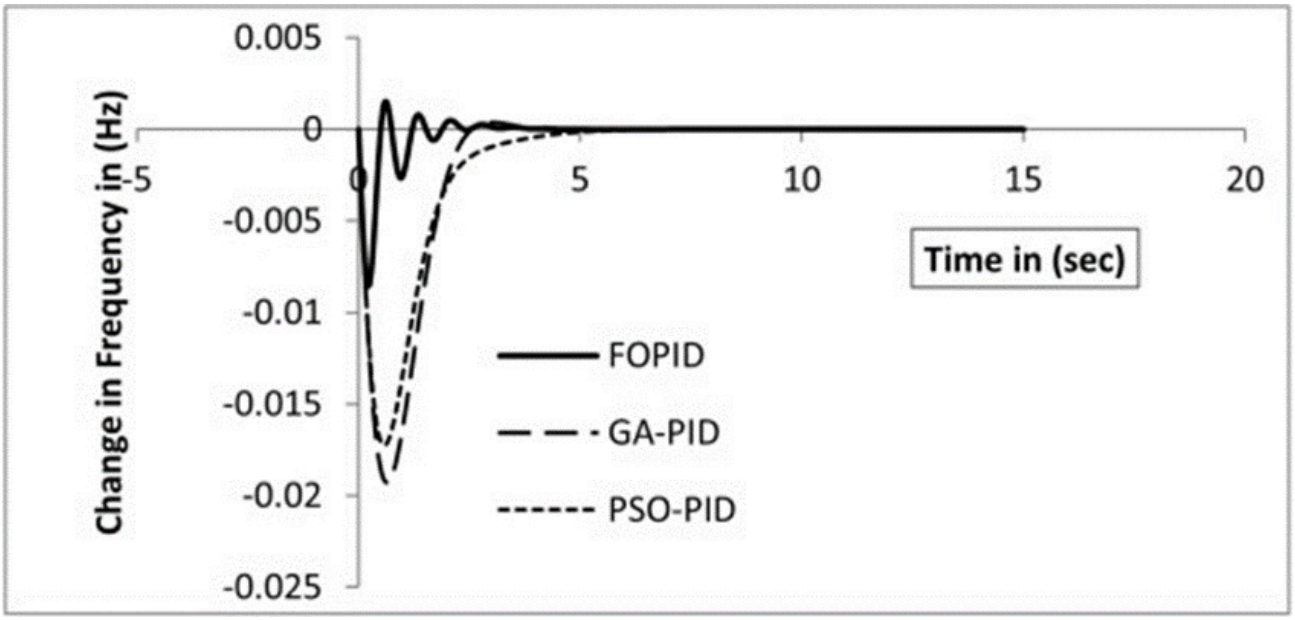


Figure 6. Transient performance comparisons of single-area AC microgrid system without DES.

© 2026 The Author(s). | Published by Institute of Smart Energy Systems Press

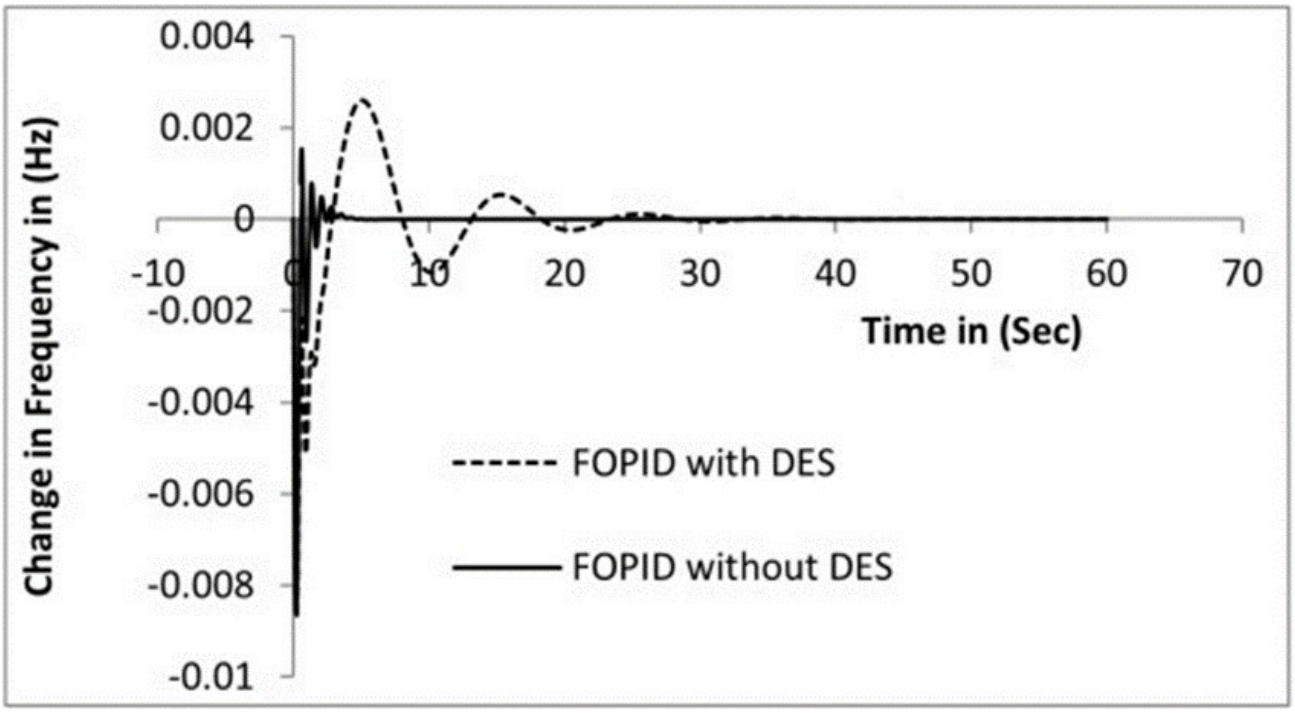
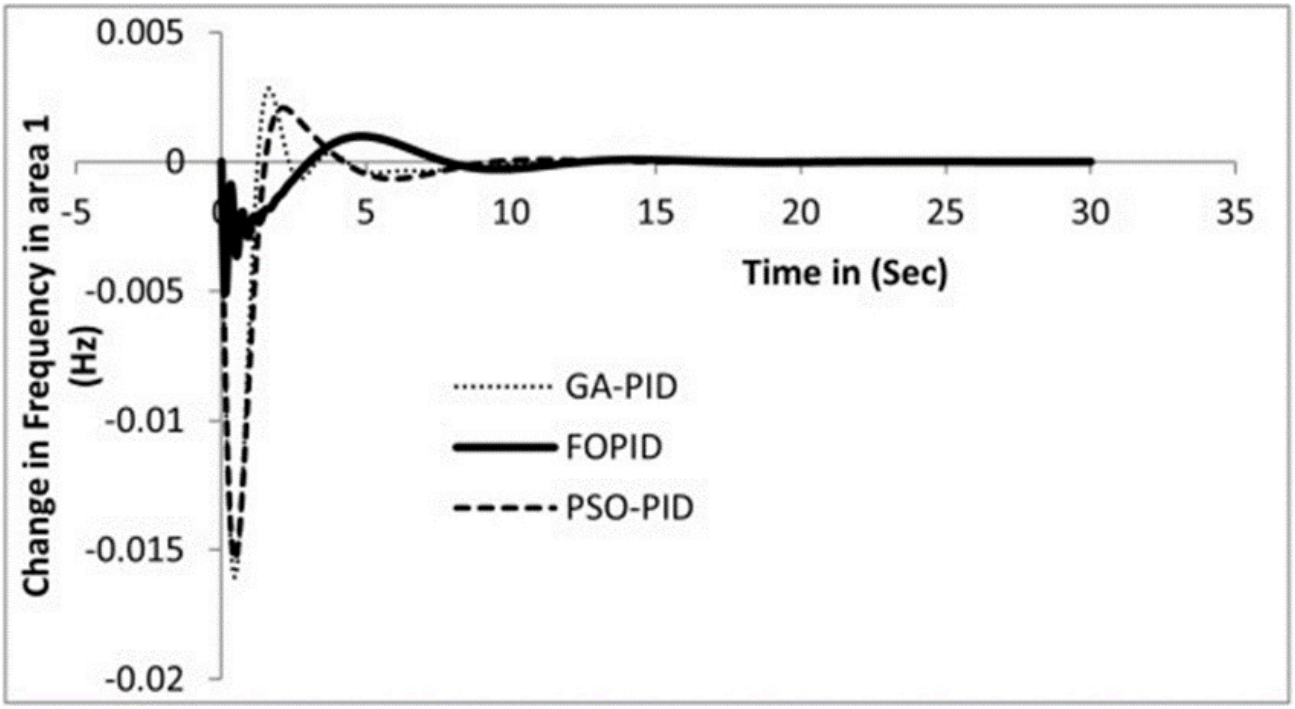


Figure 7. Transient analysis of single-area AC microgrid with and without DES (Distributed Energy System).

Case 2. Load changes in a two-area AC microgrid system

Within the interconnected dual-area AC microgrid, frequency shifts were categorized as Δf1 in area 1, Δf2 in area 2, and ΔPtie12 across the interconnecting tie-line. **Figures 8 and 9** illustrate the system's reaction to a 0.01 p.u. MW disturbance introduced in areas 1 and 2, respectively. These visualizations clearly demonstrate that configurations governed by the FOPID controller experience substantially mitigated oscillations relative to the PSO-PID and GA-PID setups, while concurrently preserving an excellent degree of steady-state accuracy. Similar performance improvements are reflected in the frequency response profiles of the dual-area tie-line, as presented in **Figure 10.**



© 2026 The Author(s). | Published by Institute of Smart Energy Systems Press

Figure 8. Frequency inconsistency in area 1 of a two-area AC microgrid power system.

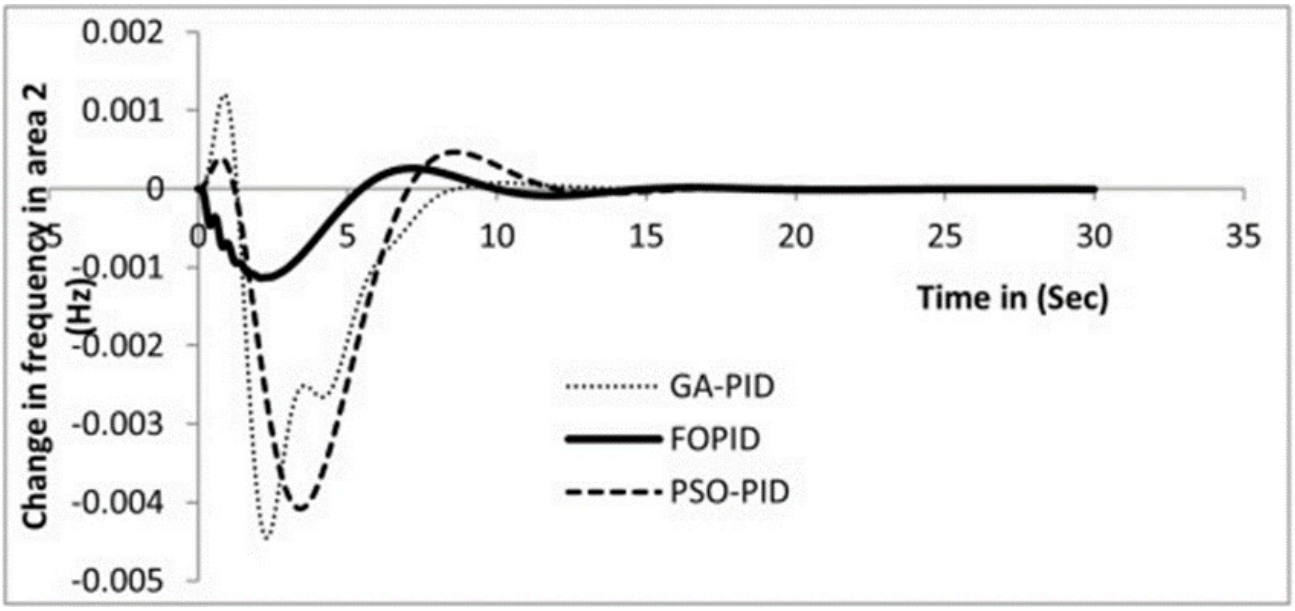


Figure 9. Frequency inconsistency in area 2 of a two-area AC microgrid power system.

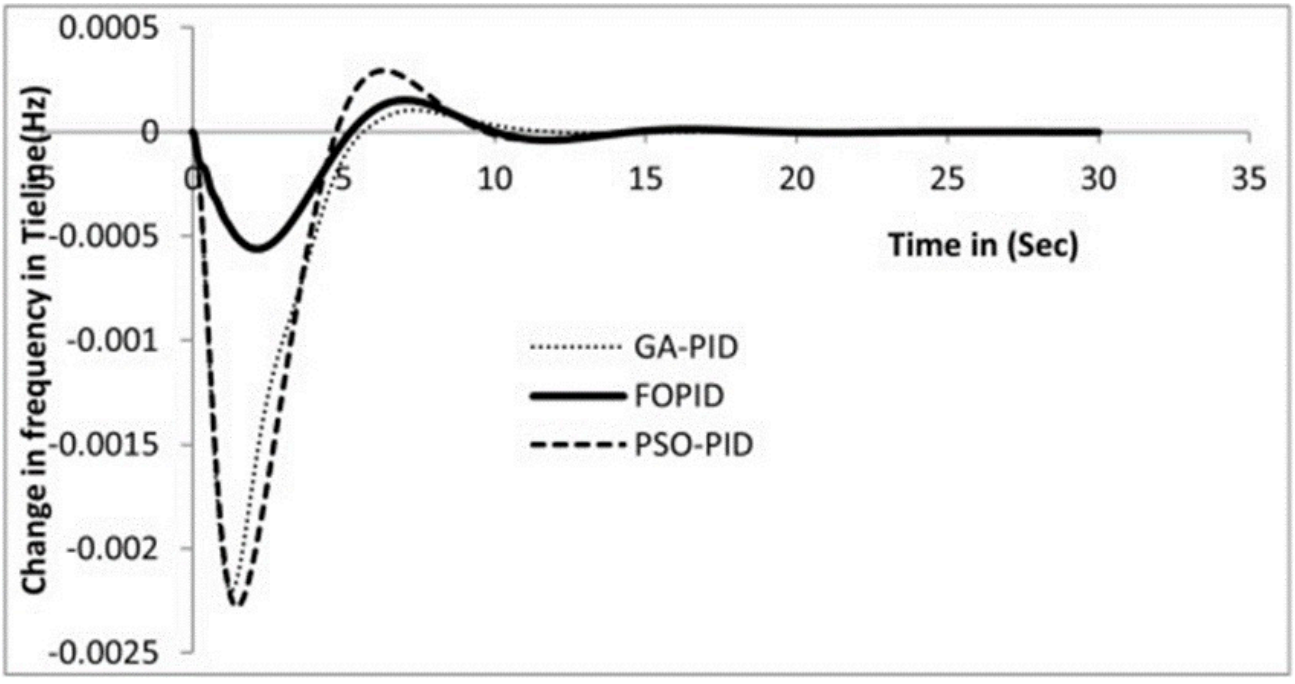


Figure 10. Frequency inconsistency in the tie line of a two-area AC microgrid power system.

Case 3. Random step load variation

The regulatory frequency responses of the FOPID-integrated LFC were subsequently evaluated under the duress of randomized step-load disturbances, mapped for both the single-area and dual-area AC microgrid frameworks in **Figures 11 and 12**, respectively. The profound regulatory impact of the FOPID mechanism within the LFC is proven by its ability to rigidly confine fluctuations within acceptable standard tolerances. Notably, the FOPID architecture exhibits vastly superior tracking accuracy when confronted with stochastic step-load variations, as visibly charted in **Figure 13** for area 1, area 2, and the tie-line.

© 2026 The Author(s). | Published by Institute of Smart Energy Systems Press

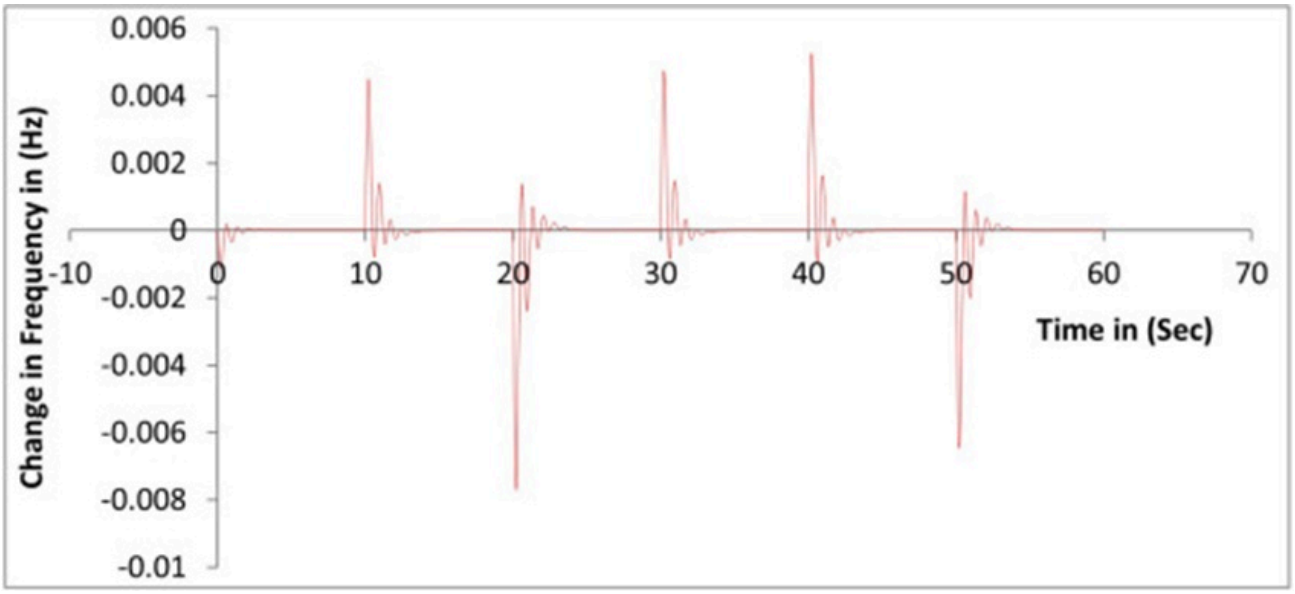


Figure 11. Performance of single-area AC micro system for random step load input.

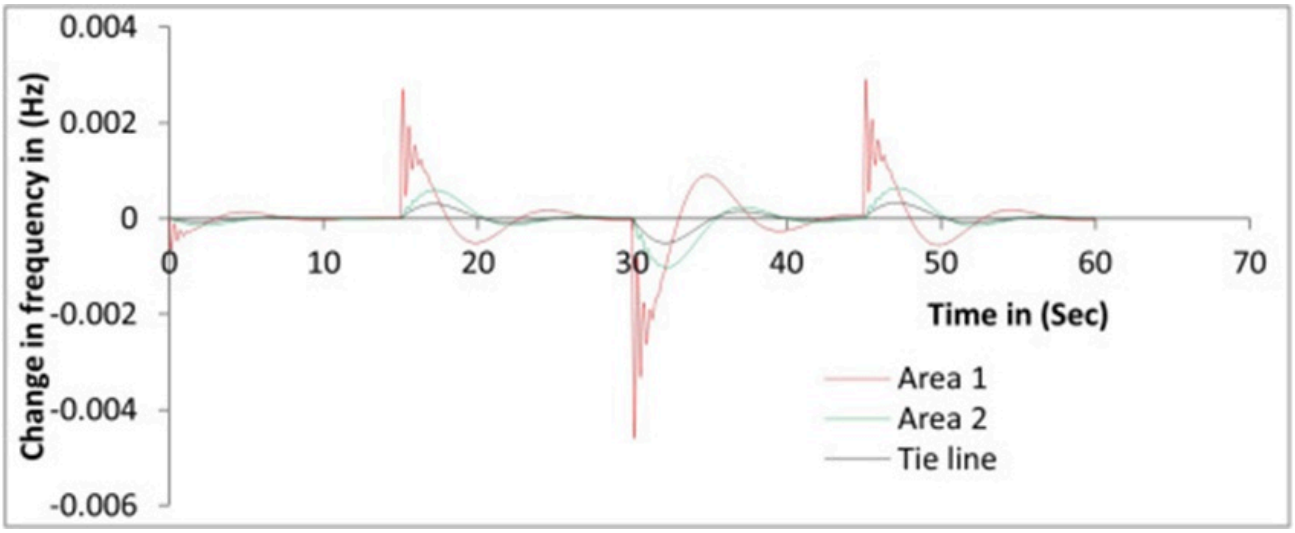


Figure 12. Performance of two-area AC micro system for random step load input.

© 2026 The Author(s). | Published by Institute of Smart Energy Systems Press

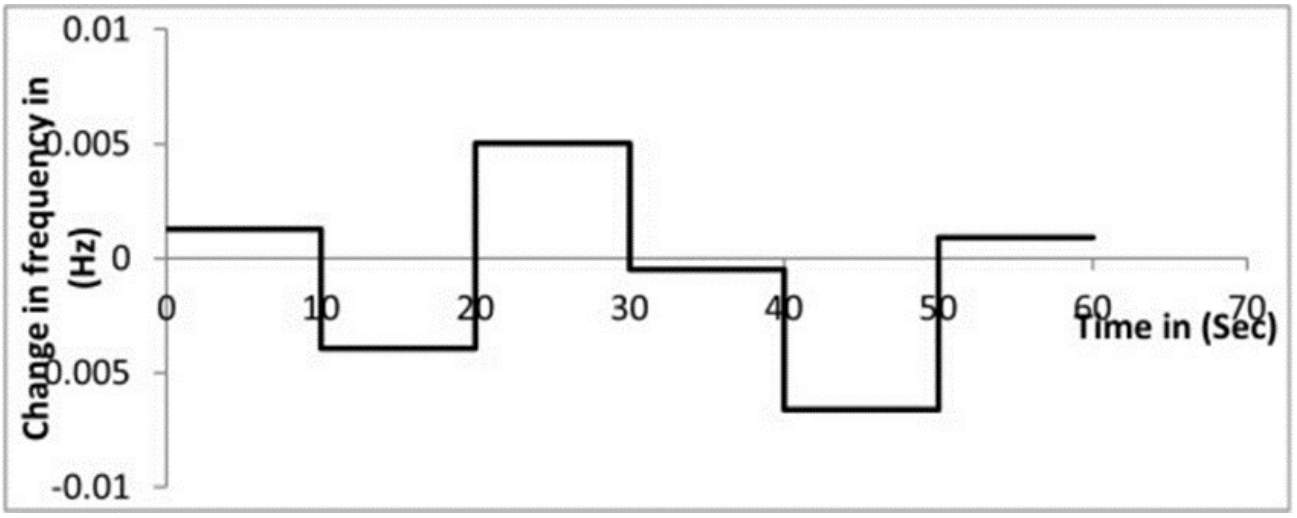


Figure 13. Input of random step load for proposed system.

Case 4. System parameter variation

To validate the inherent robustness of the introduced AC microgrid FOPID controller, core operating time constants (Tg, Tg1, and Tg2) were manipulated to be (i) 25% and 50% above, and (ii) 25% and 50% below their established baseline values. Even under these drastic deviations, the optimized FOPID gain metrics remained largely stable, as documented in **Table 5**. Likewise, the specific FOPID gain parameters did not experience drastic shifts when subjected to corresponding alterations in microgrid system benchmarks. This is specifically evidenced by the frequency deviations at the single-area PCC point (Δf) responding to concurrent step-load changes at the PCC (Δf) scaling between 0.1 p.u and 1.0 p.u, thoroughly outlined in **Table 5**. Based on these analyses, it is clear that the FOPID-governed system maintains consistent output characteristics regardless of large fluctuations in foundational power system parameters.

The consolidated empirical data presented across **Tables 2-5** definitively prove that the advocated FOPID controller curtails oscillatory behavior and enhances steady-state precision (via shorter settling times) far better than conventional LFC auxiliary regulators tuned via particle swarm or genetic algorithms. Synthesizing these outcomes, it is reasonable to conclude that deploying a FOPID controller is the optimal method for securing the absolute lowest magnitude of overshoots/undershoots and the briefest possible settling periods. The structural robustness exhibited by this fractional-order LFC mechanism—particularly when defending against both fixed and randomized step-load disturbances—firmly reinforces its elite operational profile.

Table 5. Robustness of FOPID controller over system parameter variations.

Robustness assessment	Variation	Undershoot (p.u. Hz)	Overshoot (p.u. Hz)	Settling Time (s)	ITAE
Nominal condition	1% SLP	−0.0085	0.0015	4.8	0.02567
	2% SLP	−0.0170	0.0030	5.0	0.00591
Load perturbation	5% SLP	−0.0430	0.0075	5.1	0.01480
	10% SLP	−0.0860	0.0150	5.1	0.02960
System parameter variations	−25%	−0.0080	0.0003	7.5	0.00222
	+25%	−0.0090	0.0027	6.5	0.00526
	−50%	−0.00727	0.0002	7.5	0.00220

© 2026 The Author(s). | Published by Institute of Smart Energy Systems Press

	+50%	−0.0095	0.0004	9.3	0.01112

Conclusion

Within this study, the operational parameters of a FOPID controller were mathematically isolated and computationally optimized utilizing the socio-inspired cohort intelligence methodology. This calibrated controller was then directly integrated as the secondary LFC loop within a theorized microgrid power architecture. The functional performance of this FOPID unit was directly benchmarked against evolutionary (GA) and swarm-based (PSO) PID regulators executing identical LFC tasks. This comparison analyzed error metrics (specifically ITAE), steady-state precision (measured by settling time), and iso-damping proficiency (evaluated via maximum overshoots and undershoots) under both randomized and standard step-load disruptions. Ultimately, the analytical findings assert that an LFC network anchored by a fractional order-proportional integral derivative controller exhibits strong resilience to parametric fluctuations and effectively mitigates severe load perturbations.

Prospective research pathways in this domain point toward investigating short-memory fractional derivatives, which promise to significantly slash computational overhead and conserve system memory [56-58]. Further academic exploration should also integrate deep learning methodologies into FOPID structural design, alongside accommodating discrete-time scenarios [59] and unpredictable environmental variables. Down the line, investigations into load frequency regulation for DC microgrids—particularly those intersecting with ocean-based or flight-control architectures utilizing hybrid fuzzy PID/fuzzy FOPID controllers—will be executed, placing a specific emphasis on achieving zero steady-state frequency errors.

Acknowledgements

None

Conflict of interest

The authors declare the following financial interests/personal relationships which may be considered as potential competing interests: MURUGESAN D reports that administrative support was provided by Paavai Engineering College. Murugesan D reports a relationship with Paavai Engineering College that includes: employment.

Financial support

None

Ethics statement

None

Received: 14 Sep 2024 Revised: 19 Nov 2024 Accepted: 06 Dec 2024
Published online: 15 June 2026

© 2026 The Author(s). | Published by Institute of Smart Energy Systems Press

Rights and permissions

Open Access The author(s) retain copyright. This article is licensed under the Creative Commons Attribution-NonCommercial-ShareAlike 4.0 International License. It may be shared and adapted for non-commercial purposes with appropriate attribution, an indication of changes, and distribution of adaptations under the same license. Third-party material may be subject to separate terms identified in its credit line. View the license at https://creativecommons.org/licenses/by-nc-sa/4.0/.

References

1. Elgerd OI, Fosha CE. Optimum megawatt-frequency control of multiarea electric energy systems. IEEE Trans Power Appar Syst. 1970;89(4):556-63.

2. Ismayil C, Sreerama KR, Sindhu TK. Automatic generation control of single area thermal power system with fractional order () controllers. IFAC Proc. 2014;47(1):552-7.

3. Topno PN, Chanana S. Fractional order PID control for LFC problem of a hydro-thermal power system. In: 2016 11th International Conference on Industrial and Information Systems (ICIIS). IEEE; 2016. p. 867-72. https://doi.org/10.1109/ICIINFS.2016.8263060.

4. Jagatheesan K, Anand B, Dey N, Ashour AS. Effect of SMES unit in AGC of an interconnected multi-area thermal power system with ACO-tuned PID controller. In: Advances in Applied Metaheuristic Computing. 2018. p. 164-84.

5. Jagatheesan K, Anand B, Dey N, Omar M, Balas VE. AGC of multi-area interconnected power systems by considering different cost functions and Ant Colony Optimization technique based PID controller. Intell Decis Technol. 2017;11(1):29-38.

6. Murugesan D, Jagatheesan K, Boopathi D. Meta-heuristic strategy planned controller for frequency supervision of integrated thermal plant with renewable source. In: 2021 PhD Research in Microelectronics and Electronics (PRIME). IEEE; 2021. p. 1-2. https://doi.org/10.1109/PhDEDITS53295.2021.9649544.

7. Ahuja A, Narayan S, Kumar J. Robust FOPID controller for load frequency control using Particle Swarm Optimization. In: 2014 6th IEEE Power India International Conference (PIICON). IEEE; 2014. p. 1-6. https://doi.org/10.1109/POWERI.2014.7117663.

8. Gorripotu TS, Samalla H, Rao JM, Azar AT, Pelusi D. TLBO algorithm optimized fractional-order PID controller for AGC of interconnected power system. In: Soft Computing in Data Analytics. Singapore: Springer; 2019. p. 847-55.

9. Gheisarnejad M, Khooban MH. Design an optimal fuzzy fractional proportional integral derivative controller with derivative filter for load frequency control in power systems. Trans Inst Meas Control. 2019;41(9):2563-81.

10. Kanimozhi R. Load frequency control of three area power system using optimal tuning of fractional order proportional integral derivative controller with multi objective grey wolf optimization. J Eng Res. 2022. https://doi.org/10.36909/jer.15090.

11. Debbarma S, Dutta A. Utilizing electric vehicles for LFC in restructured power systems using fractional order controller. IEEE Trans Smart Grid. 2016;8(6):2554-64.

12. Bingul Z, Karahan O. Comparison of PID and FOPID controllers tuned by PSO and ABC algorithms for unstable and integrating systems with time delay. Optim Control Appl Methods. 2018;39(4):1431-50.

13. Kaliannan J, Baskaran A, Dey N, Ashour AS. Bio-inspired algorithms in PID controller optimization. Boca Raton: CRC Press; 2018.

14. Mishra D, Sahu PC, Prusty RC, Panda S. A fuzzy adaptive fractional order-PID controller for frequency control of an islanded microgrid under stochastic wind/solar uncertainties. Int J Ambient Energy. 2021;:1-10.

© 2026 The Author(s). | Published by Institute of Smart Energy Systems Press

https://doi.org/10.1080/01430750.2021.1990137.

15. Arya Y. A new optimized fuzzy FOPI-FOPD controller for automatic generation control of electric power systems. J Franklin Inst. 2019;356(11):5611-29.

16. Ismayil C, Kumar RS, Sindhu TK. Optimal fractional order PID controller for automatic generation control of two-area power systems. Int Trans Electr Energy Syst. 2015;25(12):3329-48.

17. Debnath MK, Agrawal R, Tripathy SR, Choudhury S. Artificial neural network tuned PID controller for LFC investigation including distributed generation. Int J Numer Model. 2020;33(5):e2741. https://doi.org/10.1002/jnm.2741.

18. Eshetu W, Sharma P, Sharma C. ANFIS based load frequency control in an isolated micro grid. In: 2018 IEEE International Conference on Industrial Technology (ICIT). IEEE; 2018. p. 1165-70.

19. Karanam AN, Shaw B. A new two-degree of freedom combined PID controller for automatic generation control of a wind integrated interconnected power system. Prot Control Mod Power Syst. 2022;7(1):1-16.

20. Debbarma S, Saikia LC. Effect of fractional-order controller on automatic generation control of a multi-area thermal system. In: 2011 International Conference on Energy, Automation, and Signal (ICEAS). IEEE; 2011.

21. Delassi A, Arif S, Mokrani L. Load frequency control problem in interconnected power systems using robust fractional () controller. Ain Shams Eng J. 2018;9(1):77-88.

22. Vijayakumar V. Approximate controllability results for analytic resolvent integro-differential inclusions in Hilbert spaces. Internat J Control. 2018;91(1):204-14.

23. Vijayakumar V, Panda SK, Nisar KS, Baskonus HM, Ravichandran C, Murugesu R, et al. Results on approximate controllability results for second-order Sobolev-type impulsive neutral differential evolution inclusions with infinite delay. Numer Methods Partial Differential Equations. 2021;37(2):1200-21.

24. Mahmudov NI, Vijayakumar V, Murugesu R. Approximate controllability of second-order evolution differential inclusions in Hilbert spaces. Mediterr J Math. 2016;13(5):3433-54.

25. Raja MM, Vijayakumar V, Udhayakumar R. A new approach on approximate controllability of fractional evolution inclusions of order 1<r<2 with infinite delay. Chaos Solitons Fractals. 2020;141:110340. https://doi.org/10.1016/j.chaos.2020.110340.

26. Raja MM, Vijayakumar V, Udhayakumar R. Results on the existence and controllability of fractional integro-differential system of order 1<r<2 via measure of noncompactness. Chaos Solitons Fractals. 2020;139:110028. https://doi.org/10.1016/j.chaos.2020.110028.

27. Kavitha K, Vijayakumar V, Udhayakumar R, Ravichandran C, Murugesu R, Panda SK, et al. Results on controllability of Hilfer fractional differential equations with infinite delay via measures of noncompactness. Asian J Control. 2022;24(3):1406-15.

28. Shah P, Agashe SD, Singh AP. Design of fractional order controller for undamped control system. In: 2013 Nirma University International Conference on Engineering (NUiCONE). IEEE; 2013. p. 1-5.

29. Shah P, Agashe S. Design and optimization of fractional PID controller for higher order control system. In: International Conference of IEEE ICART. 2013. p. 588-92.

30. Çelik E. Design of new fractional order PI–fractional order PD cascade controller through dragonfly search algorithm for advanced load frequency control of power systems. Soft Comput. 2021;25(2):1193-217.

© 2026 The Author(s). | Published by Institute of Smart Energy Systems Press

31. Fayek HH. Load Frequency Control of a Power System with 100% Renewables. In: 2019 54th International Universities Power Engineering Conference (UPEC). IEEE; 2019. p. 1-6. https://doi.org/10.1109/UPEC.2019.8893587.

32. Babaei M, Abazari A, Muyeen SM. Coordination between demand response programming and learning-based FOPID controller for alleviation of frequency excursion of hybrid microgrid. Energies. 2020;13(17):4426. https://doi.org/10.3390/en13174426.

33. Sondhi S, Hote YV. Fractional order PID controller for load frequency control. Energy Convers Manage. 2014;85:343-53.

34. Khokhar B, Dahiya S, Parmar KS. A novel fractional order proportional integral derivative plus second-order derivative controller for load frequency control. Int J Sustain Energy. 2021;40(3):235-52.

35. Mahto T, Malik H, Mukherjee V, Alotaibi MA, Almutairi A, Sharma G, et al. Renewable generation based hybrid power system control using fractional order-fuzzy controller. Energy Rep. 2021;7:641-53.

36. Shah P, Kulkarni AJ. Application of variations of cohort intelligence in designing fractional PID controller for various systems. In: Socio-Cultural Inspired Metaheuristics. Singapore: Springer; 2019. p. 175-92.

37. Shah P, Agashe S, Kulkarni AJ. Design of a fractional () controller using the cohort intelligence method. Front Inf Technol Electron Eng. 2018;19(3):437-45.

38. Sekhar R, Shah P. Predictive modeling of a flexible robotic arm using cohort intelligence socio-inspired optimization. In: 2020 1st International Conference on Information Technology, Advanced Mechanical and Electrical Engineering (ICITAMEE). IEEE; 2020. p. 193-8.

39. Murugesan D, Shah P, Jagatheesan K, Sekhar R, Kulkarni AJ, Nair SS, et al. Cohort intelligence optimization based controller design of isolated and interconnected thermal power system for automatic generation control. In: 2022 Second International Conference on Computer Science, Engineering and Applications (ICCSEA). IEEE; 2022. p. 1-6.

40. Özdemir MT, Öztürk D, Eke İ, Çelik V, Lee KY. Tuning of optimal classical and fractional order PID parameters for automatic generation control based on the bacterial swarm optimization. IFAC-PapersOnLine. 2015;48(30):501-6.

41. Khan A, Khan H, Gómez-Aguilar JF, Abdeljawad T. Existence and Hyers-Ulam stability for a nonlinear singular fractional differential equations with Mittag-Leffler kernel. Chaos Solitons Fractals. 2019;127:422-7.

42. Khan H, Gomez-Aguilar JF, Abdeljawad T, Khan A. Existence results and stability criteria for ABC-fuzzy-Volterra integro-differential equation. Fractals. 2020;28(08):2040048. https://doi.org/10.1142/S0218348X20400484.

43. Alkhazzan A, Jiang P, Baleanu D, Khan H, Khan A, Shah R, et al. Stability and existence results for a class of nonlinear fractional differential equations with singularity. Math Methods Appl Sci. 2018;41(18):9321-34.

44. Tajadodi H, Khan ZA, Gómez-Aguilar JF, Khan A, Khan H, Ilyas A, et al. Exact solutions of conformable fractional differential equations. Results Phys. 2021;22:103916. https://doi.org/10.1016/j.rinp.2021.103916.

45. Khan A, Alshehri HM, Gómez-Aguilar JF, Khan ZA, Fernández-Anaya G, Shah K, et al. A predator–prey model involving variable-order fractional differential equations with Mittag-Leffler kernel. Adv Difference Equ. 2021;2021(1):1-18.

46. Sekhar R, Singh T, Shah P. Machine learning based predictive modeling and control of surface roughness generation while machining micro boron carbide and carbon nanotube particle reinforced Al-Mg matrix composites. Particul Sci Technol. 2022;40(3):355-72.

© 2026 The Author(s). | Published by Institute of Smart Energy Systems Press

47. Sekhar R, Singh T, Shah P. Micro and nano particle composite machining: Fractional order control of surface roughness. In: Proceedings of the Third International Conference on Powder, Granule and Bulk Solids: Innovations and Applications (PGBSIA). 2020. p. 35-42.

48. Sekhar R, Singh TP, Shah P. Complex order PI d design for surface roughness control in machining CNT Al-Mg hybrid composites. Adv Sci Technol Eng Syst J. 2020;5(6):299-306.

49. Warrier P, Shah P. Optimal fractional PID controller for buck converter using cohort intelligent algorithm. Appl Syst Innov. 2021;4(3):50.
https://doi.org/10.3390/asi4030050.

50. Warrier P, Shah P. Fractional order control of power electronic converters in industrial drives and renewable energy systems: a review. IEEE Access. 2021;9:58982-9009.

51. Shah P, Sekhar R. Predictive modeling and control of clamp load loss in bolted joints based on fractional calculus. In: Advances in Computing and Network Communications. Singapore: Springer; 2021. p. 15-32.

52. Shah P, Sekhar R, Iswanto I, Shah M. Complex order PID controller design for a fractional order DC motor system. Adv Sci Technol Eng Syst J. 2021;6(2):541-51.

53. Shah P, Sekhar R, Agashe S. Application of fractional PID controller to single and multi variable non minimum phase systems. Int J Recent Technol Eng. 2019;8(2):2801-11.

54. Shah P, Sharma D, Sekhar R. Analysis of research trends in fractional controller using latent Dirichlet allocation. Eng Lett. 2021;29(1):197-206.

55. Shah P, Agashe S. Review of fractional PID controller. Mechatronics. 2016;38:29-41.

56. Kilbas AA, Srivastava HM, Trujillo JJ. Theory and applications of fractional differential equations. Vol. 204. Amsterdam: Elsevier; 2006.

57. Wu GC, Kong H, Luo M, Fu H, Huang LL. Unified predictor–corrector method for fractional differential equations with general kernel functions. Fract Calc Appl Anal. 2022;25(2):648-67.

58. Wu GC, Zeng DQ, Baleanu D. Fractional impulsive differential equations: exact solutions, integral equations and short memory case. Fract Calc Appl Anal. 2019;22(1):180-92.

59. Wu GC, Wei JL, Luo C, Huang LL. Parameter estimation of fractional uncertain differential equations via Adams method. Nonlinear Anal Model Control. 2022;27(2):1-15.

© 2026 The Author(s). | Published by Institute of Smart Energy Systems Press